Journal of Power Sources 180 (2008) 63–70

Contents lists available at ScienceDirect

Journal of Power Sources

journal homepage: www.elsevier.com/locate/jpowsour

# Functionalized carbon nanotube-poly(arylene sulfone) composite membranes for direct methanol fuel cells with enhanced performance

Sang Hoon Joo[a], Chanho Pak[a], Eun Ah Kim[a], Yoon Hoi Lee[a], Hyuk Chang[a], Doyoung Seung[a], Yeong Suk Choi[a,*], Jong-Bong Park[b], Tae Kyoung Kim[c]

[a] Energy & Environment Laboratory, Samsung Advanced Institute of Technology, P.O. Box 111, Suwon, 440-600, Republic of Korea
[b] Analytical Engineering Center, Samsung Advanced Institute of Technology, P.O. Box 111, Suwon, 440-600, Republic of Korea
[c] Research Institute of Chemical & Electronic Materials, Cheil Industries Inc., Uiwang-si, 437-711, Republic of Korea

ARTICLE INFO

*Article history:*
Received 24 October 2007
Received in revised form 19 January 2008
Accepted 1 February 2008
Available online 16 February 2008

*Keywords:*
Polymer electrolyte membrane
Carbon nanotubes
Poly(arylene sulfone)s
Composites
Direct methanol fuel cell (DMFC)
Power density

ABSTRACT

A new type of composite membrane, consisting of functionalized carbon nanotubes (CNTs) and sulfonated poly(arylene sulfone) (sPAS), is prepared for direct methanol fuel cell (DMFC) applications. The CNTs modified with sulfonic acid or PtRu nanopaticles are dispersed within the sPAS matrix by a solution casting method to afford $SO_3$CNT-sPAS or PtRu/CNT-sPAS composite membranes, respectively. Characterization of the composite membranes reveals that the functionalized CNTs are homogeneously distributed within the sPAS matrix and the composite membranes contain smaller ion clusters than the neat sPAS. The composite membranes exhibit enhanced mechanical properties in terms of tensile strength, strain and toughness, which leads to improvements in ion conductivity and methanol permeability compared with the neat sPAS membrane. In DMFC performance tests, the use of a PtRu/CNT-sPAS membrane yields high power density compared with the neat sPAS membrane, which demonstrates that the improved properties of the composite membranes induce an increase in power density. The strategy for CNT-sPAS composite membranes presented in this work can potentially be extended to other CNT-polymer composite systems.



## 1. Introduction

The direct methanol fuel cell (DMFC) is considered to be a promising power source for next-generation portable electronic devices that require high power densities and long operation times. This is because the DMFC has high specific energy, low emission of greenhouse gas, convenience in refuelling, and ambient operation condition [1–3]. There are, however, many obstacles to be overcome for the commercialization of DMFC as a power source. Critical issues to be addressed include slow reaction kinetics at the anode and methanol crossover from the anode to the cathode. In particular, the latter problem, which is mainly related to the diffusion behaviour of methanol in polymer electrolyte membranes (PEMs) [4–7], results in a decrease in potential at the cathode and a loss of fuel efficiency. To date, perfluorosulfonic acid (PFSA) membranes, Nafion® being a representative example, are the most prevalent PEMs for fuel cell applications, due to their high ion conductivities, good mechanical properties and high chemical stabilities. The PFSA-type membranes, however, exhibit a considerable degree of methanol crossover. To decrease the methanol crossover, several strategies have been pursued. These include the use of hydrocarbon-based membranes that are resistant to methanol crossover [6,7] and the modification of PEMs with metal oxides or metals as functional moieties [7].

The hydrocarbon-based membranes have been widely investigated as alternatives to the PFSA-type membranes due to their relatively low methanol permeability and low production cost. Representative hydrocarbon membranes are poly(ether ketone)s, poly(arylene ether sulfone)s, poly(imide)s and poly(phosphazene)s [6]. For DMFC applications of hydrocarbon-based membranes, a high degree of sulfonation is required to endow high ion conductivity which, however, concomitantly provokes a decrease in mechanical stability and an increase in methanol crossover. Alternatively, organic-inorganic composite membranes have been prepared by adding inorganic functional entities, such as silica, titania, zirconia, zirconium phosphates, clays, zeolites and Pd metal, into PEMs to reduce methanol crossover and to enhance mechanical strength [8–18]. Unfortunately, these composite membranes possess the drawback of low ion conductivity. This is because hydrophilic inorganic entities strongly interact with the sulfonic acid group in PEMs, which leads to the inhibition of effective ion transport through membranes. Overall, although considerable

* Corresponding author. Tel.: +82 31 280 9326; fax: +82 31 280 9359.
*E-mail address:* yeongsuk.choi@samsung.com (Y.S. Choi).

0378-7753/$ – see front matter © 2008 Elsevier B.V. All rights reserved.
doi:10.1016/j.jpowsour.2008.02.014

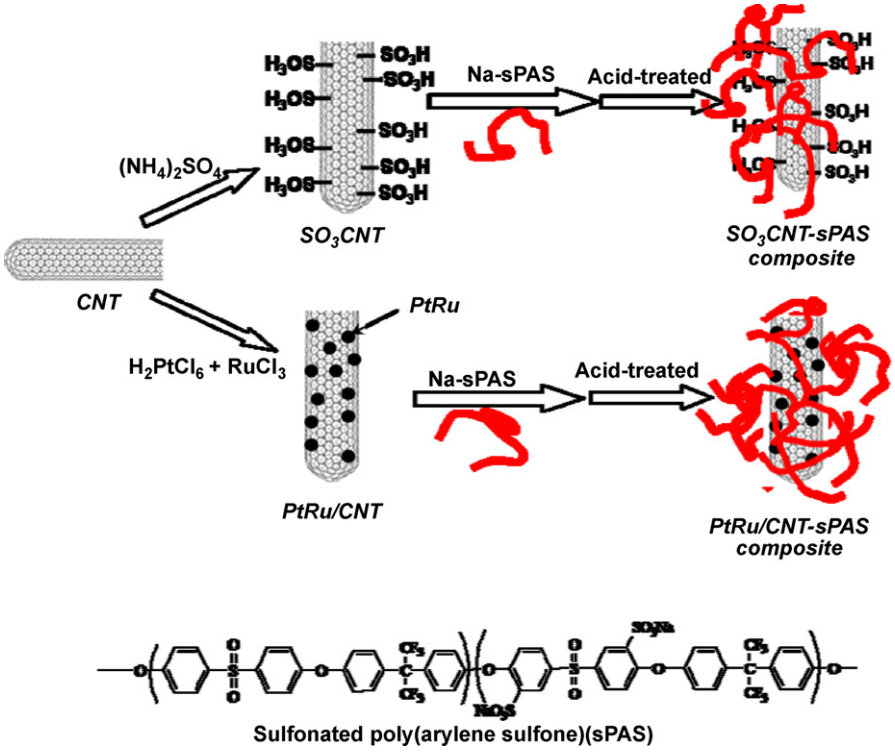


**Fig. 1.** Schematic representation of functionalized CNTs and functionalized CNT-sPAS composite membranes.

research effort has been devoted to the development of new PEMs with enhanced physicochemical properties, the preparation of PEMs exhibiting both high mechanical strength and ion conductivity still remains a challenging subject.

Carbon nanotubes (CNTs), which consist of single or several graphene layers, have attracted much attention as a reinforcing material for polymers, due to their low densities, high aspect ratios and remarkable mechanical properties [19–23]. Research results on CNT-reinforced polymer composites have shown that physical properties, such as tensile moduli and strength, are affected by the amount of nanotubes and their state of dispersion (or alignment) within polymer matrices [23]. Secondary force interactions and stress/deformations arising from mismatching coefficients of thermal expansion between CNTs and polymers were suggested as governing factors for CNT-polymer matrix adhesion. To date, however, despite the aforementioned advantageous properties, CNT-incorporated composite membranes have not been exploited for DMFC applications.

In the present work, a new type of composite membrane, in which functionalized CNTs are dispersed in a sulfonated poly(arylene sulfone) (sPAS) matrix, is prepared for DMFC applications. The preparation scheme of the new composite membranes is presented in Fig. 1. A multi-walled CNT is functionalized to have sulfonic acid groups or PtRu nanoparticles on the surface that are expected to act as ion transport sites or scavengers of methanol diffusing through membranes, respectively. The modified CNTs are dispersed in a sPAS solution, and the mixtures are fabricated into thin film membranes by a solution casting method. The final composite membranes are designated as $SO_3$CNT-sPAS and PtRu/CNT-sPAS, respectively. The CNTs dispersed in the composite membranes can interact with the aromatic groups of sPAS via secondary interaction forces (non-covalent $\pi$–$\pi$ interactions, electrostatic interactions, and van der Waals interactions) that may enable homogeneous distribution of the CNTs without blocking ion conductive sulfonic acid sites in the sPAS matrix.

## 2. Experimental

### 2.1. Preparation of functionalized CNTs

The sulfonic acid functionalized CNTs, i.e., $SO_3$CNTs, were prepared by following the method of Xu et al. [24] in which ammonium sulfate salt ($(NH_4)_2SO_4$) was used as the source of sulfonic acid. The nominal content of sulfonic acid groups was controlled at 20 wt.%. The CNTs modified with PtRu nanoparticles, PtRu/CNTs, were prepared by incipient wetness impregnation of metal precursors and subsequent reduction under a hydrogen flow. Briefly, 0.0915 g of $H_2PtCl_6{\cdot}xH_2O$ (Umicore, 40 wt.% Pt) and 0.0475 g of $RuCl_3{\cdot}xH_2O$ (Umicore, 40 wt.% Ru) were simultaneously dissolved in 1.5 mL of acetone. The metal precursor solution was slowly added 0.5 g of the multi-walled CNTs (NanoKorea Co., Korea), and the mixture was vigorously agitated until the precursor solution was completely adsorbed. After being dried in an oven at 333 K overnight, the impregnated CNTs were heated to 523 K in a $H_2$ flow and kept for 2 h at that temperature. Adsorbed hydrogen was removed by heating the PtRu impregnated CNTs under nitrogen flow at 623 K for 2 h. The nominal loading of PtRu was 10 wt.%.

### 2.2. Synthesis of sPAS

sPAS was synthesized by following a method described elsewhere [25–27]. 4,4′-dichlorodiphenyl sulfone (TCI, 0.0095 mole), sulfonated 4,4′-dichlorodiphenyl sulfone (sodium form, 0.0105 mole), hexafluoroisopropylidiene diphenol (Aldrich, 0.0204 mole), and potassium carbonate (Aldrich) were used for condensation polymerization. *N*-Methyl-2-pyrrolidinone and toluene were used for polymerization solvents. Water, formed during the aromatic substitution reaction, was removed with toluene through azeotropic distillation at 423 K and, subsequently, the polymerization was carried out at 453 K for 6 h. The synthesized polymer, sodium form sPAS (Na-sPAS), was recovered by precipitating the

reactants into methanol and then washing three times with de-ionized water.

### 2.3. Preparation of functionalized CNT-sPAS composite membranes

For the preparation of composite membranes, surface functionalized CNTs (1 wt.% to Na-sPAS) was added into Na-sPAS solution (10 wt.% in *N*,*N*′-dimethylacetamide, DMAc), and the mixture solution was sonicated for 1 h, followed by stirring for more than 12 h. The dispersions were cast on glass plates, and dried at 333 K for 12 h. To convert the membranes into the proton form (sPAS), the composite membranes were treated with 1 M·$H_2SO_4$ aqueous solution at 368 K for 2 h and then washed with de-ionized water until any excess of sulfonic acid was completely removed.

### 2.4. Characterization

The tensile strength of the membrane was measured with a Tinius Olsen UTM H5K-T universal testing machine. Each membrane was prepared in a size of 5 mm (width) × 30 mm (length). The distance between the two grips of UTM was fixed at 10 mm and the drawing speed of the grips was set at 50 mm $min^{-1}$.

Ion conductivity was evaluated by a four-point probe method using a Solartron 1260 a.c. impedance analyzer with an amplitude of 20 mV and a frequency range of 1 Hz–500 kHz. Each membrane (1.5 × 4.0 cm) was fitted in a Teflon conductivity test cell that consisted of two Pt wires (a counter electrode and a working electrode) and two Pt foils (reference electrode 1 and reference electrode 2). The Teflon test cell was immersed in a de-ionized water bath to maintain the membrane at constant humidity and temperature. Membrane resistance was calculated using the intercept value of the real axis ($Z'$) in the complex plane that is composed of the real axis and the imaginary axis ($Z''$). Ionic conductivity was calculated via the following equation:

$$\sigma = \left(\frac{1}{R}\right)\left(\frac{L}{A}\right) \quad (1)$$

where $R$ is the resistance, $L$ is the length, and $A$ is the cross-sectional area of a membrane.

Methanol permeability was measured using a diffusion cell that consisted of two reservoirs. A membrane with a transporting area of 10 $cm^2$ was placed between a methanol reservoir and a water reservoir. The internal volume of each reservoir was 35 ml. Methanol permeability was calculated using the following equation which describes the relationship between methanol concentrations and elapsed times [28–31].

$$P = \left(\frac{\Delta C_B}{\Delta t}\right)\left(\frac{1}{C_{Ai}}\right)\left(\frac{L}{A}\right)V_B \quad (2)$$

where $P$ is the permeability of a membrane; $\Delta C_B/\Delta t$ is the slope of a molar concentration variation of methanol in the water reservoir as a function of time; $C_{Ai}$ is the initial concentration of methanol in its reservoir; $L$ and $A$ are the thickness and the area of a membrane, respectively; $V_B$ is the volume of de-ionized water in its reservoir.

The metal content in PtRu/CNTs was analyzed by a Shimadzu ICPS-8100 inductively coupled plasma atomic emission spectrometer (ICP-AES). The ICP-AES was calibrated with a series of three standard solutions containing 0, 5 and 50 ppm of Pt prepared in 10 wt.% HCl background solution. Transmission electron microscope (TEM) images were taken using a FEI TECNAI F20 $G^2$ scanning transmission electron microscope at an accelerating voltage of 200 kV. Energy-dispersive X-ray spectroscopy (EDX) analysis was performed with the TECNAI F-30 at an accelerating voltage of 300 kV. For observing the dispersion states and particle sizes of ion

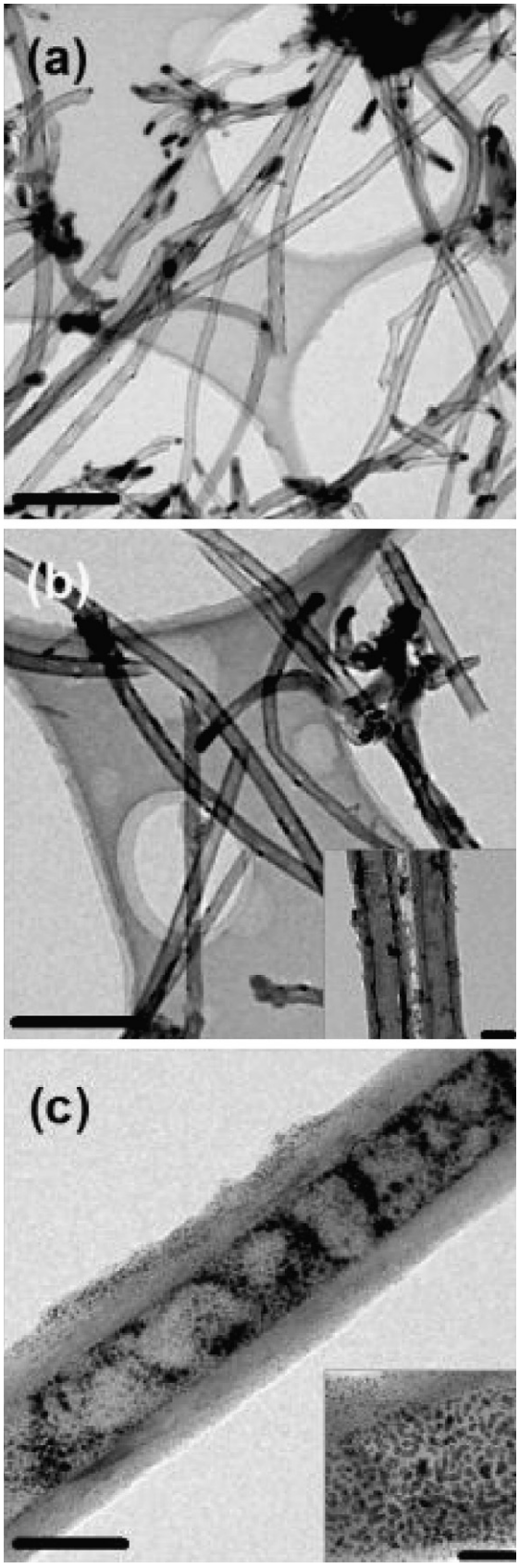


**Fig. 2.** TEM images of pristine CNT and functionalized CNTs. (a) Pristine CNT, scale bar, 500 nm; (b) $SO_3$CNT, scale bar, 500 nm (inset: high magnification image; scale bar, 50 nm); (c) PtRu/CNT; scale bar, 50 nm (inset: high magnification image; scale bar, 20 nm).

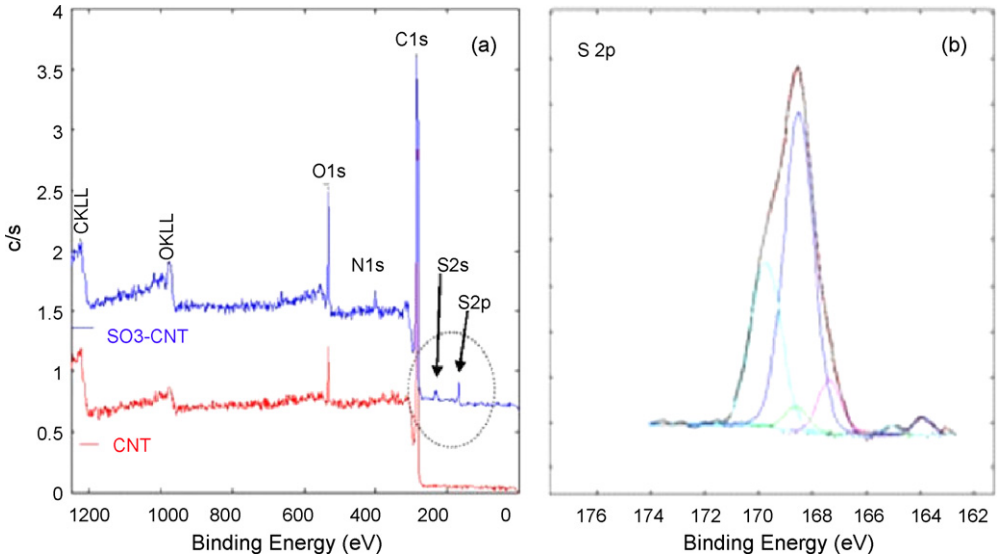


**Fig. 3.** XPS spectra of pristine and functionalized CNT samples. (a) Survey spectra of $SO_3$CNT (blue) and pristine CNT (red) and (b) S 2p region spectrum of $SO_3$CNT (For interpretation of the references to colour in this figure legend, the reader is referred to the web version of the article).

clusters in membranes, membranes were stained with 0.5 M silver nitrate aqueous solution by the procedure described elsewhere [32]. Stained membranes were moulded with epoxy resin and sliced to yield samples of about 90 nm in thickness using a RMC Powertome XL ultramicrotome. Finally, the sliced samples were placed on copper grids. X-ray photoelectron spectroscopy (XPS) measurements were conducted using a PHI Q2000 X-ray photoelectron spectrometer, equipped with a monochromatized Al Kα (1486.6 eV) source. Thermogravimetric analyses (TGA) were performed using a Perkin-Elmer TGA-7 instrument from room temperature to 973 K with a ramping rate of 10 K per min under a nitrogen atmosphere. UV absorbance spectra were collected using a Varian Cray 5000 UV–vis spectrometer at room temperature. UV absorbance was scanned from 190 to 500 nm [33,34].

### 2.5. Evaluation of DMFC performance [35]

For the fabrication of membrane-electrode assembly (MEA), a cathode catalyst ink was prepared by treating a commercial Pt black catalyst (HiSpec 1000 from Johnson Matthey Fuel Cells) with a Nafion® dispersion in alcohol solution. The catalyst ink was coated on to a gas-diffusion layer to form a cathode catalyst layer with a Pt loading of 5 mg $cm^{-2}$. An anode catalyst layer was prepared by loading 5 mg $cm^{-2}$ of PtRu black catalyst (HiSpec 6000 from Johnson Matthey Fuel Cells, Pt:Ru ratio = 1:1) on the gas-diffusion layer based on the same method for the cathode catalyst layer. A membrane was placed between the cathode and anode catalyst layers and hot-pressed to fabricate MEAs with a reaction area of 10 $cm^2$. DMFC performance tests were conducted with a single cell at 333 K with 1 M methanol aqueous solution (anode fuel) and dry air (cathode fuel, oxidant), respectively, which were fed at a 3 stoichiometric rate.

## 3. Results and discussion

Fig. 2 shows TEM images of pristine and functionalized CNTs. The pristine CNTs, as can be seen in Fig. 2a, was composed of multi-walled nanotubes and contained metal particles that were used as the catalyst for the growth of nanotubes. The pristine CNT bundles were functionalized with sulfonic acid groups or PtRu nanoparticles, following the scheme presented in Fig. 1. $SO_3$CNTs maintained the multi-walled structures of the pristine CNTs, as seen in Fig. 2b. The TEM image of Fig. 2c shows that PtRu particles of PtRu/CNTs exhibit a size of ca. 2–3 nm and are uniformly dispersed onto the CNT bundles without significant change in the morphology of the pristine CNTs.

Qualitative and quantitative analyses for sulfonic acid groups present in the $SO_3$CNTs were performed by XPS and TGA, respectively. XPS spectra of the pristine CNTs and the $SO_3$CNTs are displayed in Fig. 3a. Unlike pristine CNTs, the $SO_3$CNTs exhibit two new peaks, S 2s and S 2p, which support the presence of S atoms in the $SO_3$CNTs. Curve fitting of the S 2p peak (Fig. 3b) reveals that the S atom exists mainly as the $SO_3^-$ form (−168.5 eV) with some portions of $SO_2$ and S–C bonding moieties. The amount of the sulfonated moiety of the $SO_3$CNTs was determined by using a weight loss difference between pristine CNTs and $SO_3$CNTs at 948 K in TGA traces (Fig. 4). The calculated $SO_3$ content of the $SO_3$CNTs is 19 wt.% (the nominal value = 20 wt.%), which indicates that the method employed in this work is effective for functionalizing CNTs.

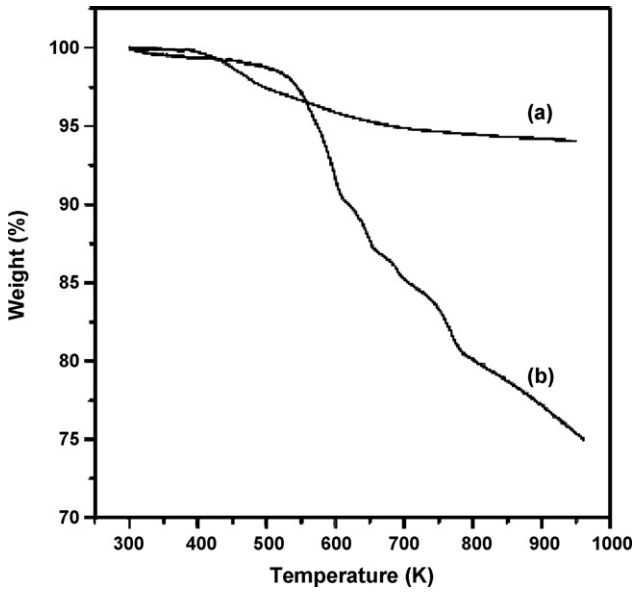


**Fig. 4.** TGA curves of (a) pristine CNT and (b) $SO_3$CNT.

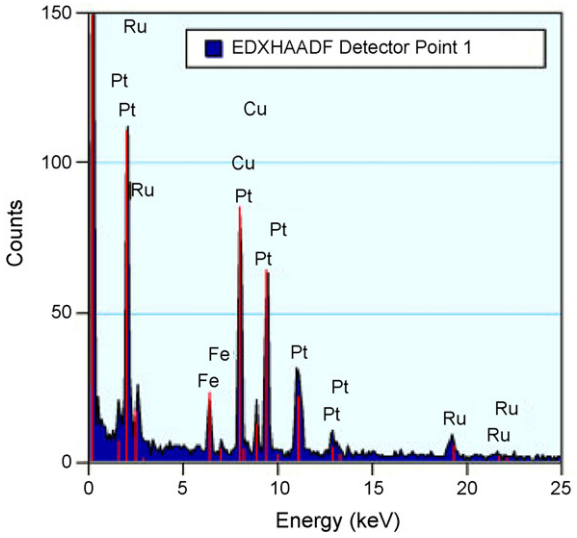


**Fig. 5.** EDX analysis of PtRu/CNT.

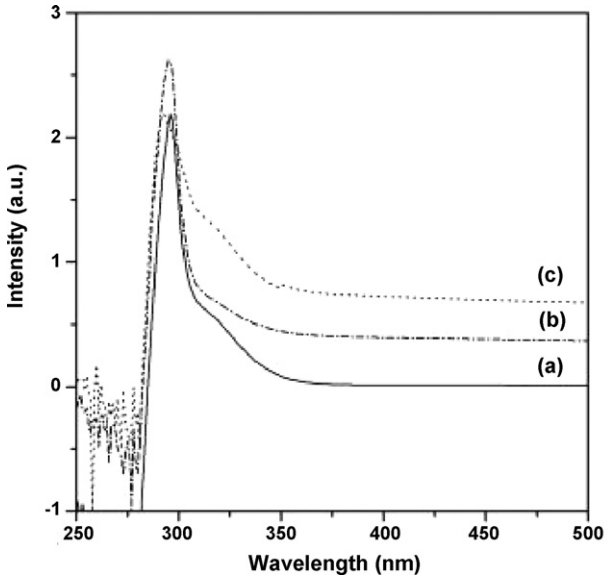


**Fig. 7.** UV absorbance spectra of (a) Na-sPAS solution in DMAc, (b) $SO_3$CNT-Na-sPAS dispersion, and (c) PtRu/CNT-Na-sPAS dispersion.

**Table 1**
ICP-AES analysis of metal contents in PtRu/CNT

| Metal | Pt | Ru | Pt + Ru |
|---|---|---|---|
| Content (wt.%) | 6.16 | 3.05 | 9.21 |
| R.S.D. (%) | 0.38 | 0.37 | 0.38 |

The PtRu nanoparticles in PtRu/CNTs were further analyzed by EDX and ICP-AES. The EDX spectrum given in Fig. 5 clearly shows the presence of Pt and Ru metals in PtRu/CNTs. Elemental analysis of the PtRu/CNT was performed by ICP-AES and the results are listed in Table 1. The amount of PtRu nanoparticles on the CNTs is 9.2 wt.% and the molar Pt:Ru ratio is 1.04, which are similar to the nominal values of 10 wt.% and 1, respectively. The characterization results indicate that the pristine CNTs are successfully modified with the functional moieties (sulfonic acid group or PtRu nanoparticles) without damage to the graphene structure or dilapidation of the bundle length.

Composite membranes are prepared with the Na-sPAS and the functionalized CNTs via a solution casting method. The Na-sPAS has a sulfonation degree of 52%, number-average molecular weight ($M_n$) of 52 958 g mole$^{-1}$, and polydispersity index ($M_w/M_n$) of 1.28. Even though both $SO_3$CNTs and PtRu/CNTs can be uniformly dispersed up to 5 wt.% in the Na-sPAS solution, the CNT content in the composite membrane is limited to 1 wt.% to avoid electrical conductivity induced by percolation of CNT bundles [36]. The photograph in the left panel of Fig. 6 shows that the functionalized CNTs are homogeneously dispersed in the Na-sPAS/DMAc solution. The dispersion states of CNTs in the Na-sPAS solution are presumably attributed to strong interactions between the two components. In the free-standing film states, the dispersion states of CNTs in the Na-sPAS matrix are maintained, as shown in the right panel of Fig. 6.

To elucidate the interactions between CNTs and the Na-sPAS matrix, UV-vis spectra of Na-sPAS and CNT-Na-sPAS dispersions in DMAc solvent were measured (Fig. 7). In previous work, the UV-vis spectroscopy was effectively used for quantitative characterization of the colloidal stability of CNT dispersions [33] and for the investigation of dispersion behaviour which have correlations with solubility parameters based on the interactions between mixtures [34]. The UV-vis spectra of CNT-Na-sPAS composites exhibit higher UV-absorbance intensity values than that of Na-sPAS, which indicates that there exist interactions between CNTs and Na-sPAS mainly via π–π bondings [36–39].

The addition of functionalized CNTs as the filler was expected to affect mechanical properties of sPAS. The cast membranes were treated with acid to convert Na-sPAS into the proton

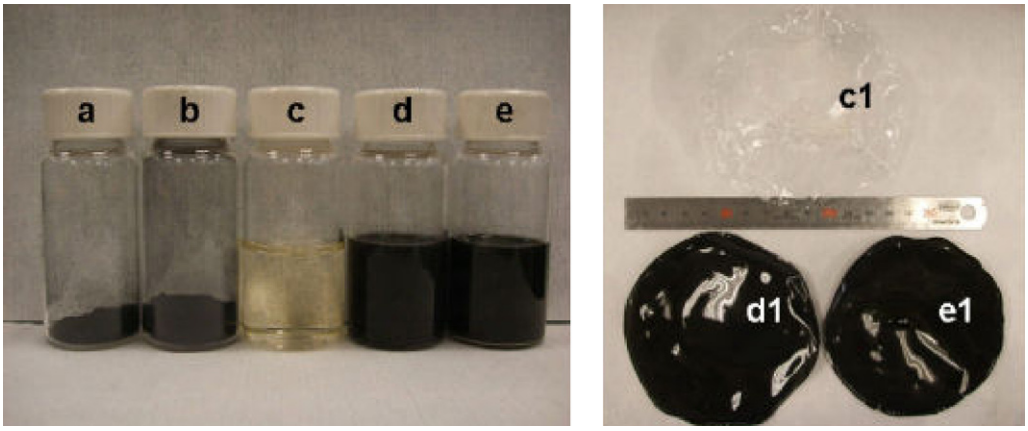


**Fig. 6.** Photographs showing dispersion states of CNTs in Na-sPAS solutions and membranes. Left: (a) $SO_3$CNT in dry state, (b) PtRu/CNT in dry state, (c) Na-sPAS solution (10 wt.% in DMAc), (d) $SO_3$CNT-Na-sPAS dispersion (1 wt.% CNT to Na-sPAS), and (e) PtRu/CNT-Na-sPAS dispersion (1 wt.% CNT to Na-sPAS). (Right) (c1) Neat sPAS membrane, (d1) $SO_3$CNT-sPAS, and (e1) PtRu/CNT-sPAS after acid treatment.

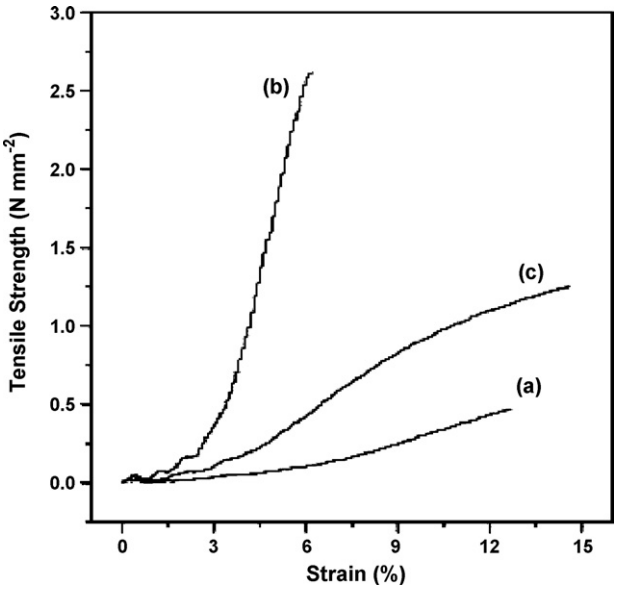


**Fig. 8.** Tensile strengths of sPAS membrane and CNT-sPAS composite membranes: (a) Neat sPAS, (b) $SO_3$CNT-sPAS, and (c) PtRu/CNT-sPAS.

form sulfonated PAS, sPAS. Fig. 8 and Table 2 present tensile strengths of CNT-sPAS composite membranes in fully hydrated states. The composite membranes display remarkable improvements in mechanical strength, exhibiting tensile strength values of 2.62 N mm$^{-2}$ for the $SO_3$CNT-sPAS and 1.25 N mm$^{-2}$ for the PtRu/CNT-sPAS, which are 457% and 165% higher than that of the neat sPAS membrane (0.47 N mm$^{-2}$). Furthermore, the CNT-sPAS composite membranes yield enhancements in toughness measurements compared with the neat sPAS membrane, as given in the following order: PtRu/CNT-sPAS (874 J m$^{-2}$, 314% higher than that of sPAS), $SO_3$CNT-sPAS (485 J m$^{-2}$, 129%), and the neat sPAS (211 J m$^{-2}$). It is well known that the mechanical property and the structural integrity of composite materials are strongly affected by interfacial structures and properties between fillers and matrixes [40]. The enhanced mechanical strength data indicate that the modified CNTs are homogeneously dispersed within the sPAS matrix without significant aggregation of the CNTs, which substantiates the interactions between CNTs and sPAS as revealed by UV-vis spectroscopy (*vide supra*).

In fuel cell membranes, ion clusters generated by aggregations of sulfonic acid groups significantly affect transport properties such as ion conductivity and methanol permeability. The effect of CNT fillers on the formation of ion clusters in the sPAS matrix was investigated by TEM. Fig. 9 shows TEM images of the neat and the composite membranes stained with 0.5 M silver nitrate aqueous solution. Proton ions in sulfonic acid groups are replaced with silver ions via ion exchange reactions during the staining process. The silver-stained ion clusters appear as dark areas due to the high electron density of silver in the TEM images. As can be seen in Fig. 9a, the neat sPAS membrane has a bimodal distribution of circular ionic clusters with sizes that are about 22 nm for large clusters and 8 nm for relatively small clusters. The $SO_3$CNT-sPAS composite membrane (Fig. 9b) has cluster sizes of 10–20 nm, which have size distribution that are more uniform than that of the pristine sPAS membrane. Furthermore, PtRu/CNT–sPAS has very uniform ion clusters of small size (4–10 nm) around the CNT walls, as displayed in Fig. 9c. The TEM images clearly show that adding the functionalized CNTs induces small, uniform sized ion clusters in the sPAS matrix. In general, it is known that decrease in ion cluster size leads to a decrease in methanol permeability [7].

Ion conductivity and methanol permeability were measured and the results are summarized in Table 2. The ion conductivity values for $SO_3$CNT-sPAS and PtRu/CNT-sPAS are 0.1 S cm$^{-1}$ and 0.106 S cm$^{-1}$, which are higher than that of the neat sPAS membrane (0.088 S cm$^{-1}$). The data indicate that the functionalization of CNTs induces an improvement in ion conductivity. Furthermore, adding functionalized CNTs to sPAS leads to a decrease in methanol permeabilities: $2.16 \times 10^{-6}$ cm$^2$ s$^{-1}$ for $SO_3$CNT-sPAS and $2.36 \times 10^{-6}$ cm$^2$ s$^{-1}$ for PtRu/CNT-sPAS, which are lower than $2.85 \times 10^{-6}$ cm$^2$ s$^{-1}$ for the sPAS membrane. The improvements in both conductivity and permeability support the discussions regarding the results from TEM observations of ion clusters.

To probe the effect of functionalized CNTs on fuel cell performance, DMFC tests were performed with single cells assembled with sPAS and PtRu/CNT-sPAS. The variation in power density in each single cell was monitored as a function of operation time. Fig. 10 presents polarization and power density curves for the DMFC single cells, which were obtained from scanning voltage tests at 60 °C. The DMFC employing the PtRu/CNT-sPAS delivers higher power densities than the single cell using the sPAS membrane. It is noteworthy that the single cell prepared with the PtRu/CNT-sPAS displayed an increase in power density with respect to operation time i.e., maximum values of 32.3 mW cm$^{-2}$ (2nd day), 45.8 mW cm$^{-2}$ (3rd day), and 54.6 mW cm$^{-2}$ (4th day). In contrast to composite membranes, the single cell employing the neat sPAS membrane gave a decrease in power density with time, i.e., maximum values of 28.5 mW cm$^{-2}$ (2nd day), 17.1 mW cm$^{-2}$ (3rd day), and 14.2 mW cm$^{-2}$ (4th day). The development of maximum power density indicates that the PtRu/CNT-sPAS exhibits better durability than that of the sPAS membrane, which may result from the uniform distribution of the CNTs in the sPAS matrix, and subsequent improvements in mechanical strength and distribution of ion clusters. Along with the enhanced power density, the single cell adopting the PtRu/CNT-sPAS show smaller changes in the slope of the polarization curves than those of the sPAS membrane-derived single cell, which manifests the low ohmic resistance (i.e., high ionic conductivity) of the PtRu/CNT-sPAS, as listed in Table 2. Furthermore, the PtRu/CNT-sPAS has a higher open-circuit voltage than that of sPAS. It is likely that the PtRu catalyst in the composite membrane scavenges methanol molecules diffusing from the anode side, so that the composite membrane sustains power density over an extended time.

Polymer electrolyte membranes containing nanometer or micrometer sized fillers have been extensively investigated for DMFC applications to address the problem of methanol crossover [7]. Various types of inorganic materials have been exploited as fillers, e.g., metal oxides, zeolites, heteropolyacids, and layered materials. Although the addition of inorganic fillers gives rise to decreases in methanol permeability, deterioration in ion conduc-

**Table 2**
Composition and mechanical and electrochemical properties of sPAS and CNT-sPAS composite membranes

| Membrane | Sulfonation degree of sPAS (%) | Modified CNT content (wt.%) | Tensile strength (max, N mm$^{-2}$) | Strain (max, %) | Toughness (J m$^{-2}$) | Conductivity (S cm$^{-1}$) | Permeability ($\times 10^{-6}$ cm$^2$ s$^{-1}$) |
|---|---|---|---|---|---|---|---|
| sPAS | 52 | 0 | 0.47 | 12.7 | 211 | 0.088 | 2.85 |
| $SO_3$CNT-sPAS | 52 | 1 | 2.62 | 6.2 | 485 | 0.100 | 2.16 |
| PtRu/CNT-sPAS | 52 | 1 | 1.25 | 14.6 | 874 | 0.106 | 2.36 |

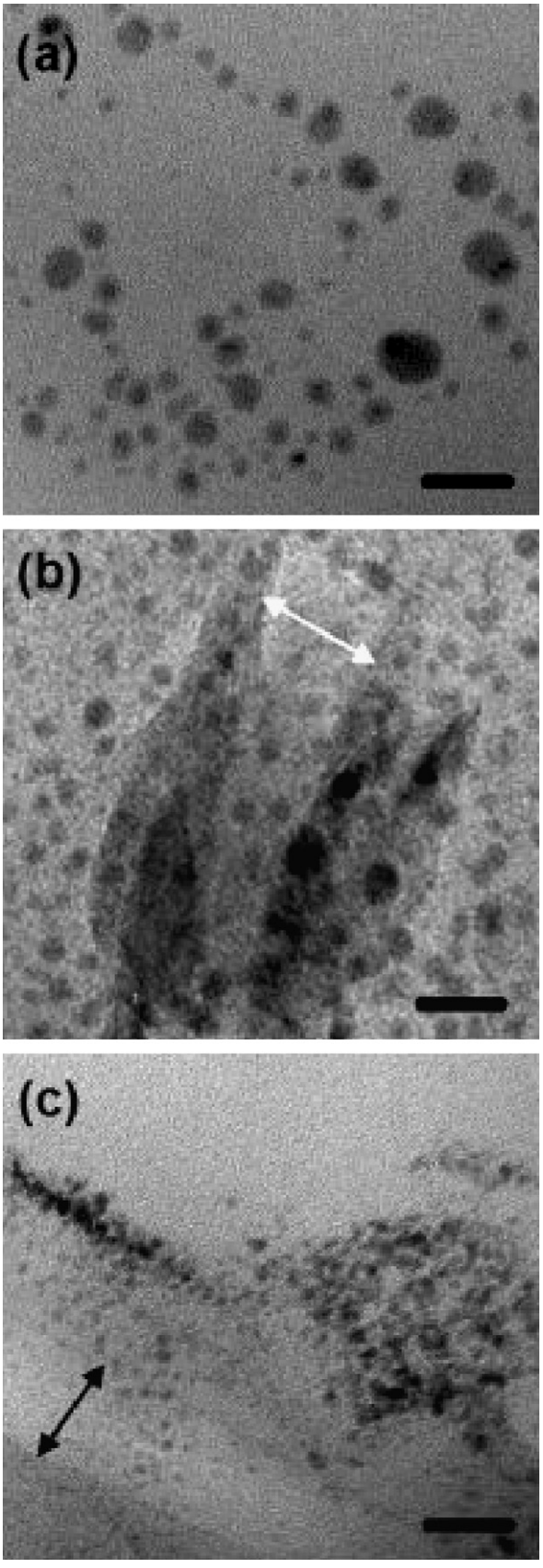


**Fig. 9.** TEM images of sPAS membrane and CNT-sPAS composite membranes. (a) Neat sPAS, (b) $SO_3$CNT-sPAS, and (c) PtRu/CNT-sPAS. Sulfonic acid groups of membranes stained with $AgNO_3$ solution [32]. Arrows of (b) and (c) indicate inside diameter of CNTs. Scale bars, 20 nm.

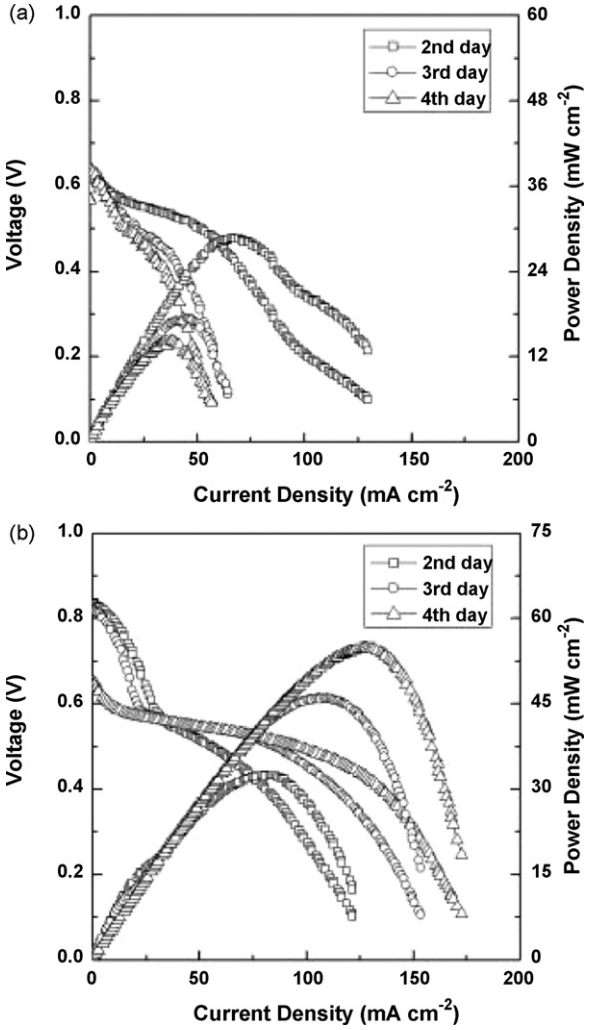


**Fig. 10.** Polarization and power density curves of DMFC single cells employing (a) neat sPAS membrane and (b) PtRu/CNT-sPAS.

tivity occurs and the membranes became brittle when the loading of fillers exceeds a certain amount. This presumably originates from the poor distribution states of fillers within polymer matrixes, due to incompatibility between the two components. In the present work, such drawbacks experienced in previous studies are avoided by introducing functionalized CNTs as the filler, as these have strong interactions with the polymer matrix, flexibility and elasticity. Consequently, the uniform distribution of CNTs within the sPAS matrix, arising from the strong interactions between the two materials, results in enhancement of mechanical and transport properties and single cell performance.

## 4. Conclusions

A new type of composite membrane, composed of functionalized CNTs and sPAS, has been prepared for DMFC applications. The functionalized CNTs homogeneously dispersed within a sPAS matrix, primarily via $\pi$–$\pi$ interactions. Adding functionalized CNTs to sPAS as a filler improves the mechanical properties in terms of tensile strength and toughness. As compared with a neat sPAS membrane, the CNT-sPAS composite membranes contain more uniform and smaller ion clusters, which results in an increase in ionic conductivity and a decrease in methanol permeability. In DMFC single-cell tests, PtRu/CNT-sPAS exhibits a low ohmic resistance and high open-circuit voltage compared with a sPAS membrane,

which collectively are believed to yield highest power densities. Furthermore, unlike the sPAS membrane, PtRu/CNT-sPAS has high durability, as evidenced by sustained power density with respect to cell operation time. The preparation of CNT-sPAS composite membranes and their application to DMFCs, as demonstrated in the present work, can potentially be extended to other CNT-polymer composite systems. In particular, recent advances in the chemistry of CNT functionalization [41] and further understanding of the interactions between CNTs and polymer matrixes may encourage the preparation of a variety of new composite materials.

## References

[1] A.S. Aricò, S. Srinivasan, V. Antonucci, Fuel Cell 1 (2001) 133–161.
[2] S.C. Thomas, X. Ren, S. Gottesfeld, P. Zelenay, Electrochim. Acta 47 (2002) 3471–3478.
[3] H. Chang, S.H. Joo, C. Pak, J. Mater. Chem. 17 (2007) 3078–3088.
[4] K.D. Kreuer, J. Membr. Sci. 185 (2001) 29–39.
[5] L. Jörissen, V. Gogel, J. Kerres, J. Garche, J. Power Sources 105 (2002) 267–273.
[6] M.A. Hickner, H. Ghassemi, Y.S. Kim, B.R. Einsla, J.E. McGrath, Chem. Rev. 104 (2004) 4587–4612.
[7] N.W. Deluca, Y.A. Elabd, J. Polym. Sci., Part B: Polym. Phys. 44 (2006) 2201–2225.
[8] P. Dimitrova, K.A. Friedrich, B. Vogt, U. Stimming, J. Electroanal. Chem. 532 (2002) 75–83.
[9] H.Y. Chang, C.W. Lin, J. Membr. Sci. 218 (2003) 295–306.
[10] B.P. Ladewig, R.B. Knott, A.J. Hill, J.D. Riches, J.W. White, D.J. Martin, J.C.D. da Costa, G.Q. Lu, Chem. Mater. 19 (2007) 2372–2381.
[11] S.P. Nunes, B. Ruffmann, E. Rikowski, S. Vetter, K. Richau, J. Membr. Sci. 203 (2002) 215–225.
[12] V.S. Silva, S. Weisshaar, R. Reissner, B. Ruffmann, S. Vetter, A. Mendes, L.M. Madeira, S. Nunes, J. Power Sources 145 (2005) 485–494.
[13] F. Bauer, M. Willert-Porada, J. Membr. Sci. 233 (2004) 141–149.
[14] C.W. Lin, R. Thangamuthu, C.J. Yang, J. Membr. Sci. 253 (2005) 23–31.
[15] D.H. Jung, S.Y. Cho, D.H. Peck, D.R. Shin, J.S. Kim, J. Power Sources 118 (2003) 205–211.
[16] C.H. Rhee, H.K. Kim, H. Chang, J.S. Lee, Chem. Mater. 17 (2005) 1691–1697.
[17] B. Libby, W.H. Smyrl, E.L. Cussler, AIChE J. 49 (2003) 991–1002.
[18] C. Pu, W. Huang, K.L. Ley, E.S. Smotkin, J. Electrochem. Soc. 142 (1995) L119–L120.
[19] C.N.R. Rao, B.C. Satishkumar, A. Govindaraj, M. Nath, ChemPhysChem 2 (2001) 78–105.
[20] J. Gao, M.E. Itkis, A. Yu, E. Bekyarova, B. Zhao, R.C. Haddon, J. Am. Chem. Soc. 127 (2005) 3847–3854.
[21] L. Liu, A.H. Barber, S. Nuriel, H.D. Wagner, Adv. Funct. Mater. 15 (2005) 975–980.
[22] S. Bellayer, J.W. Gilman, N. Eidelman, S. Bourbigot, X. Flambard, D.M. Fox, H.C. De Long, P.C. Trulove, Adv. Funct. Mater. 15 (2005) 910–916.
[23] M. Moniruzzaman, K.I. Winey, Macromolecules 39 (2006) 5194–5205.
[24] Z. Xu, Z. Qi, A. Kaufman, Electrochem. Solid-State Lett. 8 (2005) A313–A315.
[25] F. Wang, T. Chen, J. Xu, Macromol. Chem. Phys. 199 (1998) 1421–1426.
[26] P. Xing, G.P. Robertson, M.D. Guiver, S.D. Mikhailenko, S. Kaliaguine, J. Polym. Sci., Part A: Polym. Chem. 42 (2004) 2866–2876.
[27] M. Ueda, H. Toyota, T. Ouchi, J. Sugiyama, K. Yonetake, T. Masuko, T. Teramoto, J. Polym. Sci., Part A: Polym. Chem. 31 (1993) 853–858.
[28] B.S. Pivovar, Y. Wang, E.L. Cussler, J. Membr. Sci. 154 (1999) 155–162.
[29] N. Carretta, V. Tricoli, F. Picchioni, J. Membr. Sci. 166 (2000) 189–197.
[30] V. Tricoli, J. Electrochem. Soc. 145 (1998) 3798–3801.
[31] R.K. Nagarale, G.S. Gohil, V.K. Shahi, J. Membr. Sci. 280 (2006) 389–396.
[32] N. Asano, M. Aoki, S. Suzuki, K. Miyatake, H. Uchida, M. Watanabe, J. Am. Chem. Soc. 128 (2006) 1762–1769.
[33] L. Jiang, L. Gao, J. Sun, J. Colloid Interface Sci. 260 (2003) 89–94.
[34] H.T. Ham, Y.S. Choi, I.J. Chung, J. Colloid Interface Sci. 286 (2005) 216–223.
[35] T.K. Kim, M. Kang, Y.S. Choi, H.K. Kim, W. Lee, H. Chang, D. Seung, J. Power Sources 165 (2007) 1–8.
[36] D. Baskaran, J.W. Mays, M.S. Bratcher, Chem. Mater. 17 (2005) 3389–3397.
[37] M. Yang, V. Koutsos, M. Zaiser, J. Phys. Chem. B 109 (2005) 10009–10014.
[38] F. Frehill, M. in het Panhuis, N.A. Young, W. Henry, J. Hjelm, J.G. Vos, J. Phys. Chem. B 109 (2005) 13205–13209.
[39] D.M. Guldi, G.M.A. Rahman, F. Zerbetto, M. Prato, Acc. Chem. Res. 38 (2005) 871–878.
[40] D. Hull, T.W. Clyne, An Introduction to Composite Materials, second ed., Cambridge University Press, New York, 1996.
[41] D. Tasis, N. Tagmatarchis, A. Bianco, M. Prato, Chem. Rev. 106 (2006) 1105–1136.